



Enhanced energy density and extraction efficiency of polar sol-gel dielectric films with reduced residual ions

Journal:	<i>Journal of Materials Chemistry C</i>
Manuscript ID	TC-ART-08-2020-003763.R2
Article Type:	Paper
Date Submitted by the Author:	10-Nov-2020
Complete List of Authors:	Kathaperumal, Mohanalingam; Georgia Institute of Technology, School of Chemistry and Biochemistry Kim, Yunsang; Mississippi State University, Sustainable Bioproducts Johnstone, Lucas; Georgia Institute of Technology, School of Chemistry and Biochemistry Tillotson, John; Georgia Institute of Technology, School of Chemistry and Biochemistry Park, Yohan; Georgia Institute of Technology Pan, Ming-Jen; Naval Research Laboratory Perry, Joseph; Georgia Institute of Technology, School of Chemistry and Biochemistry

ARTICLE

Enhanced energy density and extraction efficiency of polar sol-gel dielectric films with reduced residual ions

Received 00th January 20xx,
Accepted 00th January 20xx

Mohanalingam Kathaperumal,^{*ab} Yunsang Kim,^{*c} Lucas R. Johnstone,^a John P. Tillotson,^a Yohan Park,^a Ming-Jen Pan^d and Joseph W. Perry^{*a}

DOI: 10.1039/x0xx00000x

We report on the effect of residual ions in dielectric sol-gel films based on 2-cyanoethyltrimethoxysilane (CNETMS) on their dielectric and energy storage properties for pulsed power applications. A wide range of pH from 1.5 to 6.5 is employed to catalyze CNETMS sol-gel films. The sol-gel films processed at near neutral pH exhibit improved dielectric and energy storage characteristics including a Weibull modulus of 11, an order of magnitude reduction of leakage current, and an extractable energy density of 32 J/cm³ with an energy extraction efficiency of 80% at 685 V/μm, as compared with the films processed at pH 1.5. These improvements are attributed to the reduced amount of ions within the sol-gel films, which is believed to suppress the detrimental effects of mobile charge carriers that are likely to trigger field-driven scattering and impact ionization, and subsequent catastrophic electrical breakdown under high electrical stress. The present work suggests the importance of engineering residual charge carriers in dielectric sol-gel films based on trifunctional alkoxy silanes for pulsed power applications.

1. Introduction

Thin films of polymer and polymer nanocomposite materials with high energy density and low loss are of great importance for pulsed power applications.¹⁻⁵ The important properties of the dielectric material for these applications include relative permittivity, breakdown strength, failure reliability, energy density, and energy extraction efficiency.⁶ Although polymeric dielectric films typically have high breakdown strength, in which the high breakdown strength of the polymers is very advantageous for commercial applications, the overall energy densities of the polymeric films suffer from low permittivity of the polymers.⁷ Recently, poly(thiourea-co-1,1-diphenylmethane) has been shown to have a maximum energy density of 22 J/cm³ with a permittivity of 4.5 and a breakdown strength of 1000 V/μm.⁸ Further, several approaches have been pursued to improve the permittivity based on polymer processing methods have greatly improved the dielectric properties of the films including energy density (< 27 J/cm³ and 51 % energy extraction efficiency).⁹ Alternative materials have also been explored for dielectric energy storage applications including polymer nanocomposites,¹⁰⁻¹³ oxide doped nanowires,^{14, 15} and multilayer polymer thin films.¹⁶⁻²⁰ Although the relative permittivity is increased in the case of polymer

nanocomposites (e.g., BaTiO₃ doped polyvinylidene fluoride copolymers), the breakdown strength of the nanocomposites is reduced significantly due to nanoparticle percolation and porosity of films.²¹

The organic-inorganic hybrid sol-gel approach is a promising method for the formation of dielectric films, as it offers relatively mild reaction conditions for the synthesis of materials with molecular-level control of composition and solution-based processing of films.²²⁻²⁴ We have recently reported on hybrid sol-gel films from 2-cyanoethyltrimethoxysilane (CNETMS) featuring a compact cyano (C≡N) dipolar group tethered to a siloxane backbone (Si-O-Si) *via* a flexible linkage as a dielectric material conferring high permittivity and high energy density. The polar cyano group in the material is believed to provide an orientational polarization mechanism which in turn imparts a high permittivity on the thin films of the hybrid material. However, performance of the CNETMS films was compromised by electrical conduction arising from charge carriers either intrinsically present or externally injected at the electric field strength above 300 V/μm.²⁵

Charge blocking layers were employed to mitigate charge carrier injection at high electric fields, which substantially improved energy extraction efficiency and energy density of the CNETMS films.^{26, 27} However, the presence of intrinsic charges in CNETMS films used to catalyze sol-gel reactions could still be problematic at high electric fields. Similarly, the negative effects of ionic impurities and associated disorder in metal oxide dielectrics and organic semiconductors have been one of the challenging research topics for optoelectronic materials.²⁸⁻³⁰

Herein, we report on the effect of residual ions on the dielectric and energy storage characteristics of the CNETMS dielectric films. To vary the amount of residual ions, *i.e.*,

^a School of Chemistry and Biochemistry, and Center for Organic Photonics and Electronics (COPE), Georgia Institute of Technology, Atlanta, GA 30332, USA. E-mail: kmohan@ece.gatech.edu; jwperry@mac.com

^b 3D Systems Packaging Research Center, Georgia Institute of Technology, Atlanta, GA 30332, USA

^c Department of Sustainable Bioproducts, Mississippi State University, 201 Locksley Way, Starkville, MS 39759, USA. E-mail: yunsang.kim@msstate.edu

^d Naval Research Laboratory, 4555 Overlook Avenue, Washington, D.C. 20375, USA

chloride ions (Cl^-) coming from 0.1 N HCl as a catalyst, CNETMS precursors were catalyzed in a wide range of pH from 1.5 to 6.5. All spin-cast CNETMS films exhibited excellent uniformity and comparable microstructure, supported by infrared spectroscopy, X-ray powder diffraction (XRD), and atomic force microscopy (AFM). Results from leakage current, breakdown strength, electric field-polarization (P-E) and charge-discharge (C-D) measurements show overall improved dielectric and energy storage performance of the CNETMS films catalyzed at pH 6.5 compared with the films catalyzed at pH 1.5, suggesting suppression of conduction loss and premature electrical breakdown triggered by residual ions combined with injected charge carriers from electrical contacts at high electric fields.

2. Experimental

2.1 Preparation and characterization of the CNETMS sol-gel films

A CNETMS sol-gel composition at pH 1.5 was prepared as reported earlier.²⁵⁻²⁷ In a typical example, a CNETMS sol, methanol, and 0.1 N HCl in the weight ratio of 1:0.5:0.5 were stirred overnight and then the mixture was spin-cast on an indium tin oxide (ITO) coated glass (ITO/glass) substrate at 5000 rpm for 30 s. After curing the spin-cast film at 130 °C for 3 hrs under vacuum, a 1 μm -thick CNETMS film was obtained. For the other films at pH >2, a gel was formed after mixing the mixture for 3 hrs (pH 6.5) or for 4 hrs (pH 3.0 and 4.8). The preformed CNETMS gel was dissolved by 30 s ultrasonication, followed by stirring after the addition of N, N-dimethylformamide (DMF) as a solvent under ambient conditions. The amount of DMF was the same to the amount of water in the mixture. After overnight stirring, the mixture was spin-coated onto an ITO/glass substrate and cured at 130 °C for 3 hrs under vacuum. The speed of spin casting was adjusted to make the thickness of CNETMS films close to 1 μm . Specifically, the spinning speed in rpm and the thickness of the associated CNETMS film were 5k and 1.06 μm , 1k and 1.2 μm , 2k and 1.04 μm , and 2k and 1.1 μm for pH 1.5, 3, 4.8, and 6.5, respectively. The thickness of the CNETMS films were determined using contact profilometry (Dektak 6M, Veeco). FTIR spectra were acquired with FTIR spectrometer (FTS7000, Agilent) equipped with an accessory for grazing incidence measurement (80 spec, Pike technologies), collecting 4000 scans for a background and 6000 for a sample at a 1 cm^{-1} resolution. The surface morphology of the bilayer films was analyzed by atomic force microscopy (ICON scanning force microscope, Bruker) in the tapping mode. Powder x-ray diffraction (XRD) data was obtained from the CNETMS films (PANalytical, X'Pert PRO Alpha-1). SEM-EDX measurements were conducted by field-emission scanning electron microscope (Zeiss Ultra60) on samples with a sputtered gold coating. Refractive index of the films was measured using a Metricon 2010 prism coupler at a wavelength of 633 nm. The films used for the measurements were spin-coated and baked at 130 °C to achieve a thickness around 2.5 μm .

2.2. Device fabrication and characterization of dielectric properties

Capacitor device structures were fabricated using CNETMS films on an ITO/glass substrate by depositing circular aluminum top electrodes (480 nm thick and areas of 0.25 and 1.0 mm^2) using a shadow mask in a thermal evaporator (PVD75, Kurt J. Lesker) at a deposition rate of 3 $\text{\AA}/\text{s}$. The capacitance and loss tangent of the single capacitor devices were measured from 100 Hz to 1 MHz at 1 V_{rms} by using an LCR meter (Agilent 4284A) and the capacitance was converted to relative permittivity, ϵ_r . The dielectric breakdown strength was measured inside a glove box (Labmaster 130, M. Braun, NH, USA) using a high-voltage supply (Keithley 248) and a probe station (H-100, Signatone, CA, USA) with a micromanipulator by sweeping the voltage from 50 V (DC) at 10 V/s up to the point of breakdown, which was indicated by a rapid increase in leakage current to over 200 μA . The electrode area used for breakdown strength measurements was 0.25 mm^2 . All dielectric permittivity and breakdown measurements were performed on at least 15 devices. Energy densities of the devices were measured by the pulsed charge-discharge (C-D) method and the polarization-electric field (P-E) method. In the C-D method, a voltage pulse with a rise time of ~ 0.5 ms, a charging time of 10 ms, and a hold time of a few hundred ms under various electric fields below the breakdown field was employed. P-E measurements were performed by a home-built modified Sawyer-Tower circuit, in which samples were subjected to voltages up to 2 kV supplied by a high voltage amplifier (Trek 610-D, Medina, NY). The induced charge on the sample was measured using a charge integrator circuit. The testing was performed using a unipolar sine waveform with a period of 10 ms. For the C-D and P-E measurements, film capacitors with an electrode area of 1 mm^2 were used. More details of both measurements can be found elsewhere.²⁶ All C-D and P-E measurements were conducted on at least 5 devices. As a sample was tested in air (not immersed in an insulating liquid), special care was taken to maintain appropriate distances (> 1 cm) between probes and cabling to avoid a flash-over.

3. Results and Discussion

Fourier transform infrared (FTIR) spectra of the powders from CNETMS films catalyzed at various pH are shown in Figure 1a. All the films exhibit strong peaks at 1030 and 1105 cm^{-1} indicating Si-O-Si asymmetric stretching bands³¹⁻³³ as well as at 2247 cm^{-1} for C \equiv N stretching, which confirmed the presence of the siloxane network with pendant cyano groups. The main difference in the FTIR spectra between the CNETMS films was seen in the intensity ratio of the two strong bands in the 1000-1300 cm^{-1} interval, *i.e.*, $R = I(1105 \text{ cm}^{-1}) / I(1030 \text{ cm}^{-1})$, which represents the condensation state of a silicate sol-gel.^{31, 34} $R < 1$ for the CNETMS film catalyzed at pH 1.5 indicates the predominance of open-chain polymeric siloxane species, whereas $R \sim 1$ for the films catalyzed at pH > 2 suggests the predominance of tetrahedral (T_n) cube like polymeric siloxane networks.^{33, 34} The microstructure of the CNETMS films was further examined by XRD in Figure 1b. XRD patterns of the sol-gel films displayed overall broad profiles, indicating the dominance of amorphous structure except the peaks ranging from 8.7° to 9.5° in 2θ , which are interpreted to reflect a

correlation distance between oxygen atoms in $\text{O}_3\equiv\text{Si}-\text{C}_2\text{H}_4-\text{CN}\cdots\text{CN}-\text{C}_2\text{H}_4-\text{Si}\equiv\text{O}_3$, as similarly reported in polyhedral silsesquioxanes $(\text{XSiO}_{1.5})_n$ derived from trifunctional alkoxy silane monomers with a substitute X.^{31, 33-35} As shown in Table 1, the correlation distance of 9.3 Å for the CNETMS film at pH 1.5 was increased to ~10.0 Å for the films at pH >2. At the same time, the band widths became narrower as pH increased, indicating a less disordered siloxane structure. Uniformity and microstructure of the CNETMS films were further examined by AFM, which showed very smooth surface profiles with RMS surface roughness in the range of 0.15 to 0.53 nm regardless of pH (Figure 2). Combined data suggest that the catalytic condition (pH) of the CNETMS films had some influence on the condensation state of siloxane networks as well as on the correlation distance between nanocrystalline domains (the separation of oxygen atoms in siloxane networks). However, the overall similarity in FTIR and XRD data as well as surface smoothness from AFM suggests that the microstructure of the CNETMS films is comparable to each other regardless of pH employed in this study.

Frequency-dependent dielectric spectra of the CNETMS films are shown in Figure 3. Relative permittivity of the films prepared at different pH did not seem to vary much as a function of pH ($\epsilon \sim 20$ @ 1 kHz). The pH-independent permittivity values of the films suggest the origin of the high permittivity to be the same that was reported earlier to be arising from the reorientational polarization of the $-\text{CN}$ group in a crosslinked siloxane network.²⁵ Loss tangent values of the films processed at different pH remained nearly constant to 0.02 from 100 to 10 kHz. A rapid rise in loss tangent above 10 kHz is believed to be the onset of dielectric resonance arising

from the reorientational polarization of the $-\text{CN}$ group, which is independent of pH. Based on the very similar trend in relative permittivity and loss tangent over a wide frequency range, we believe that the fabrication of the CNETMS films catalyzed at various pH led to the formation of almost identical crosslinked siloxane networks with tethering polar cyano pendant groups in the resultant sol-gel films.

Leakage current of the CNETMS films at various pH is shown in Figure 4a. Compared to the film catalyzed at pH 1.5, the current density, J , of the CNETMS films at pH > 2 dropped by an order of magnitude. Initial rise in the leakage current for the film at pH 1.5 (in black dots) was ascribed to the activation of mobile charges in the dielectric film,³⁶ which was clearly suppressed in the other films catalyzed at pH > 2. The possible sources of current in these films are the ions (H^+ , OH^- , CH_3O^- and Cl^-) generated from the catalyst used for the sol-gel hydrolysis and condensation, namely 0.1 N HCl (@ pH 1.5), diluted 0.1 N HCl (@ pH 3.0 and pH 4.8) and ultrapure water (@ pH 6.5). The main contribution to the leakage current is assumed to be Cl^- ions since the concentration of Cl^- ions decreases as pH increases, as shown in Figure 4b. Atomic weight percent of Cl^- from the films processed at various pH obtained by the elemental mapping in energy-dispersive X-ray spectroscopy (EDX) indicates the reduction of Cl^- ions with increasing pH, in which the atomic wt% of chlorine dropped from 9.05 at pH 1.5 to 1.28 at pH 4.8, whereas the atomic wt% of nitrogen remained unchanged. Moreover, the refractive index of the CNETMS films measured at 633 nm decreased with increasing pH (Table 2), which was also indicative to the decreased Cl^- in the CNETMS sol-gel films.³⁷

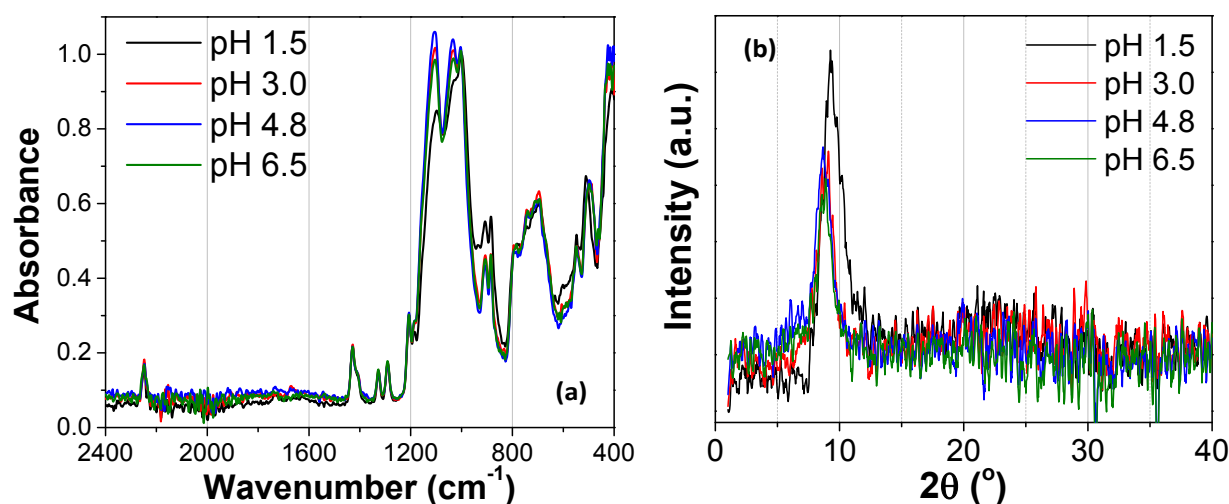


Figure 1. (a) FTIR spectra of the CNETMS films processed at various pH. (b) XRD patterns of the CNETMS films processed at different pH.

Table 1. Bragg angles (2θ), band widths (Δ in $^\circ 2\theta$), and correlation distances obtained from the XRD patterns of the CNETMS films catalyzed at various pH.

pH	2θ ($^\circ$)	Band width ($^\circ 2\theta$)	Correlation distance (\AA)
1.5	9.47	1.58	9.3
3.0	8.89	1.31	9.9
4.8	8.72	1.32	10.1

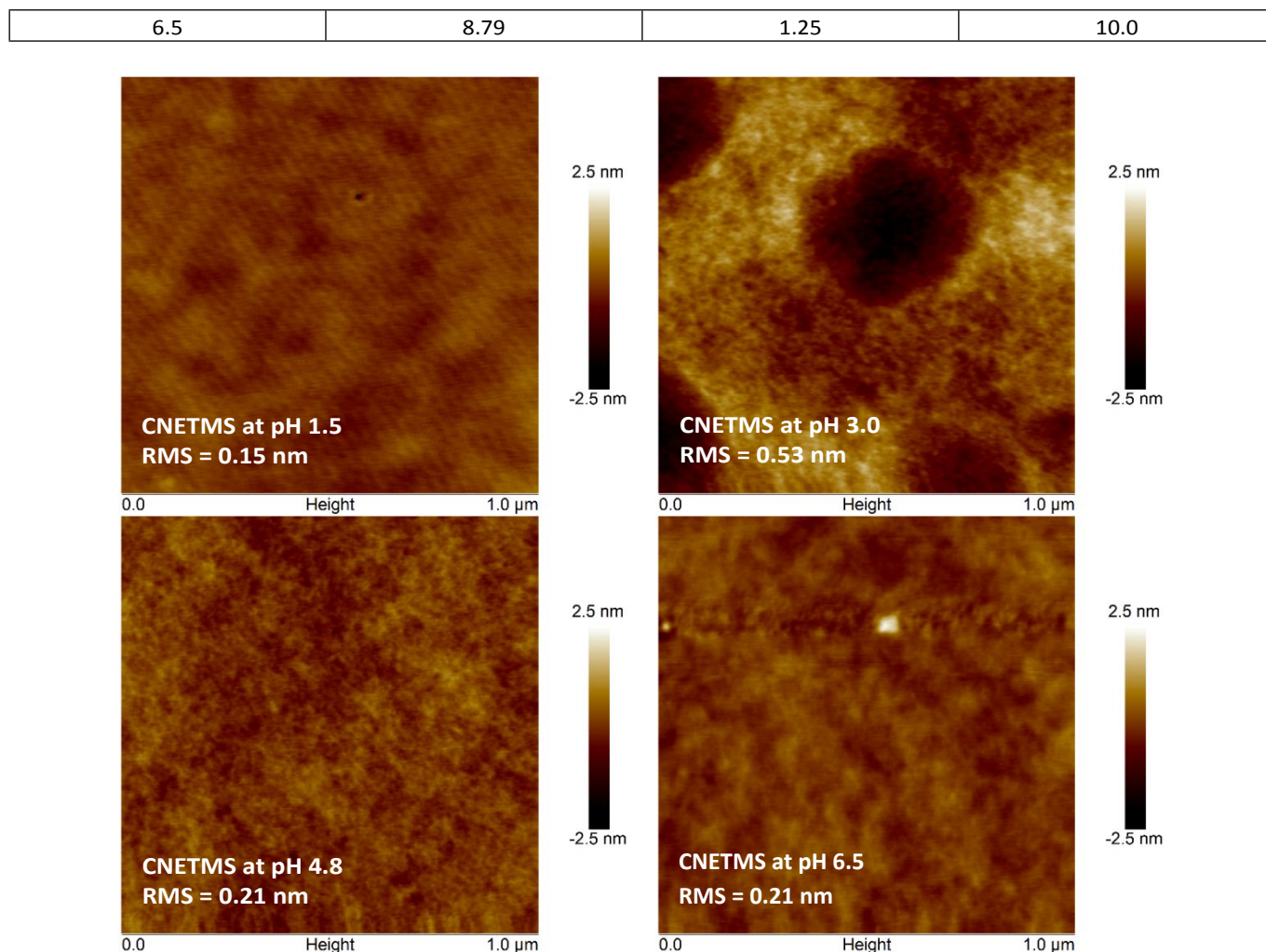


Figure 2. AFM images of the CNETMS films catalyzed at various pH with RMS surface roughness values.

Frequency-dependent dielectric spectra of the CNETMS films are shown in Figure 3. Relative permittivity of the films prepared at different pH did not seem to vary much as a function of pH ($\epsilon \sim 20$ @ 1 kHz). The pH-independent permittivity values of the films suggest the origin of the high permittivity to be the same that was reported earlier to be arising from the reorientational polarization of the $-\text{CN}$ group in a crosslinked siloxane network.²⁵ Loss tangent values of the films processed at different pH remained nearly constant to 0.02 from 100 to 10 kHz. A rapid rise in loss tangent above 10 kHz is believed to be the onset of dielectric resonance arising from the reorientational polarization of the $-\text{CN}$ group, which is independent of pH. Based on the very similar trend in relative permittivity and loss tangent over a wide frequency range, we believe that the fabrication of the CNETMS films catalyzed at various pH led to the formation of almost identical crosslinked siloxane networks with tethering polar cyano pendant groups in the resultant sol-gel films.

Leakage current of the CNETMS films at various pH is shown in Figure 4a. Compared to the film catalyzed at pH 1.5, the current density, J , of the CNETMS films at pH > 2 dropped by an order of magnitude. Initial rise in the leakage current for the film at pH 1.5 (in black dots) was ascribed to the activation

of mobile charges in the dielectric film,³⁶ which was clearly suppressed in the other films catalyzed at pH > 2. The possible sources of current in these films are the ions (H^+ , OH^- , CH_3O^- and Cl^-) generated from the catalyst used for the sol-gel hydrolysis and condensation, namely 0.1 N HCl (@ pH 1.5), diluted 0.1 N HCl (@ pH 3.0 and pH 4.8) and ultrapure water (@ pH 6.5). The main contribution to the leakage current is assumed to be Cl^- ions since the concentration of Cl^- ions decreases as pH increases, as shown in Figure 4b. Atomic weight percent of Cl^- from the films processed at various pH obtained by the elemental mapping in energy-dispersive X-ray spectroscopy (EDX) indicates the reduction of Cl^- ions with increasing pH, in which the atomic wt% of chlorine dropped from 9.05 at pH 1.5 to 1.28 at pH 4.8, whereas the atomic wt% of nitrogen remained unchanged. Moreover, the refractive index of the CNETMS films measured at 633 nm decreased with increasing pH (Table 2), which was also indicative to the decreased Cl^- in the CNETMS sol-gel films.³⁷

The dielectric breakdown strength, E_B , failure reliability (Weibull modulus, θ), and Weibull distribution of the CNETMS films are shown in Figure 5a and 5b. The details of determining θ can be found elsewhere.^{21, 26} E_B of the film catalyzed at pH 1.5 decreased initially for the film at pH 3.0, but the other films at

pH 4.8 and 6.5 marked similar values to the film at pH 1.5 with much reduced standard deviation. The increase in pH led to an increase in β , which corresponds to a decrease in the spread of breakdown strength and enhanced reliability to electrical failure, as shown in the narrower scattering of failure probability distribution in Figure 5b. Specifically, β increased from 5 to 11 when the pH changed from 1.5 to 6.5. This increase in β , which was also seen in the reduced standard deviation of E_B in Figure 5a, can be attributed to the reduced amount of ions

(most likely Cl^-) from pH 1.5 to pH 3.0 and 4.8, and then further to the absence of chloride ions at pH 6.5. The reduction of residual ions and/or ionic species in the CNETMS films seems to contribute to the enhancement of β . As shown in Figure 4a where the CNETMS films at pH >2 marked much reduced leakage currents, these ions are believed to contribute to impact ionization of accelerated mobile charge carriers particularly at high electric fields, which consequently will lead to premature breakdown of a dielectric material.³⁶

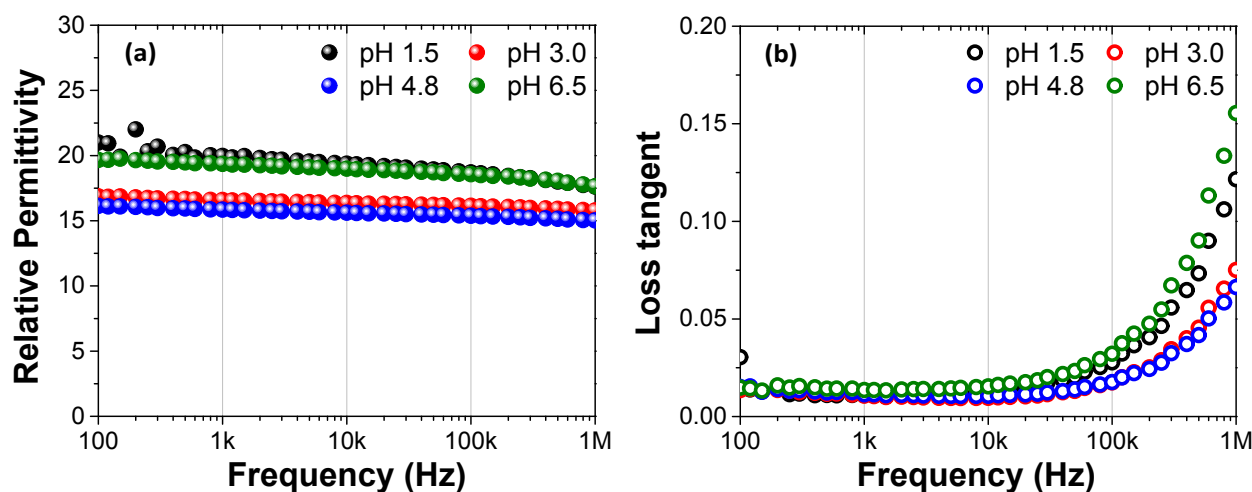


Figure 3. Frequency dependent (a) relative permittivity and (b) loss tangent of the CNETMS films catalyzed at various pH.

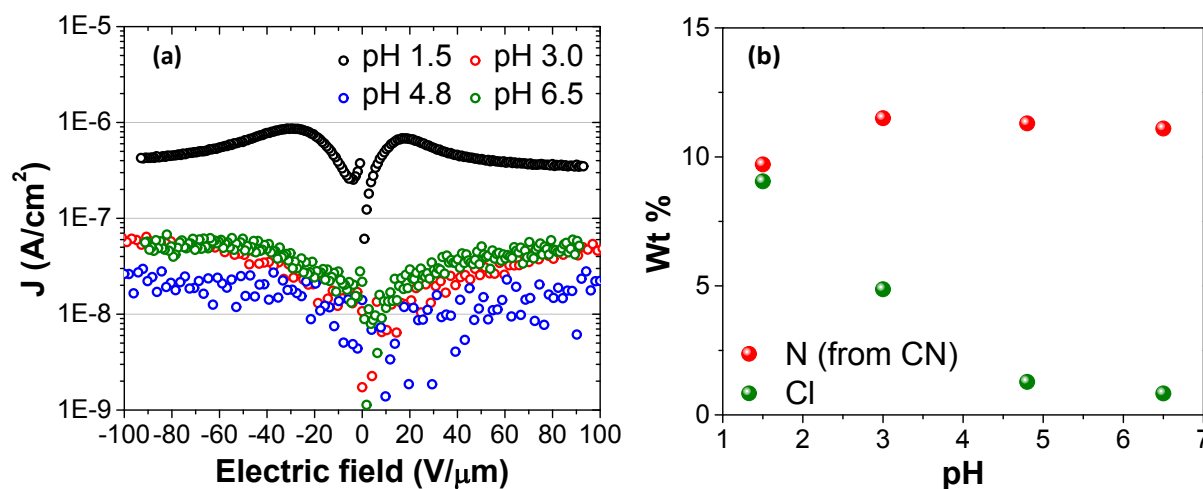


Figure 4. (a) Leakage current densities of the CNETMS films prepared at various pH. (b) Atomic weight percent of chlorine and nitrogen in the CNETMS films obtained from SEM-EDX measurements.

Table 2. Refractive index of CNETMS films catalyzed at various pH.

pH	1.5	3.0	4.8	6.5
Refractive index @ 633 nm	1.4837	1.4828	1.4824	1.4823

The field-dependent maximum extractable energy density, U_{max}^{P-E} , (shown in solid dots) and energy extraction efficiency (in hollow dots) of the CNETMS films from polarization-electric field (P-E) measurements are shown in Figure 6a. All CNETMS films displayed quadratic growth of U_{max}^{P-E} as electric field rose until dielectric breakdown. Extraction efficiency of all the films during charge-discharge cycles of P-E measurements remained

high (above 90%) up to 300 $\text{V}/\mu\text{m}$ and rapidly decreased as applied electric field increased above 300 $\text{V}/\mu\text{m}$, which can be attributed to dielectric scattering and conduction loss arising from accelerated charged species at high electric field.^{25-27, 38} Compared with the film processed at pH 1.5 (in black dots), the films catalyzed at pH >2 exhibited higher U_{max}^{P-E} and higher extraction efficiency at the same field strength. In particular, the

pH 6.5 processed film marked U_{max}^{P-E} of 32 J/cm^3 at the field strength of $680 \text{ V}/\mu\text{m}$ with energy extraction efficiency of 80%, which are shown in green solid and hollow dots. U_{max}^{P-E} of the films processed at $\text{pH} > 2$ are comparable at all field strengths below $580 \text{ V}/\mu\text{m}$ until dielectric breakdown of the individual films occurred. We believe that enhanced U_{max}^{P-E} , energy extraction efficiency, and breakdown strength field for the films processed at $\text{pH} > 2$ are attributed to the reduced amount of chloride ions with increasing pH. In particular, improved energy extraction efficiency of the films processed at $\text{pH} > 2$ suggests reduced dielectric and conduction loss arising from accelerated carriers (e.g., electrons, holes, and other impurities) under high electric fields.³⁹

The field-dependent maximum discharged energy density, U_{max}^{C-D} , of the CNETMS films from charge-discharge (C-D) measurements is shown in Figure 6b. The CNETMS films catalyzed at pH 1.5 and 4.8 exhibited a maximum energy density of 17 and 16 J/cm^3 at field strengths of 472 and $481 \text{ V}/\mu\text{m}$, respectively. However, the films from pH 3.0 and 6.5 catalyzed sols broke down at lower field strengths of 375 and $274 \text{ V}/\mu\text{m}$ and exhibited U_{max}^{C-D} of 11 and 7 J/cm^3 , respectively. Unlike the results from P-E, the CNETMS films at $\text{pH} > 2$ exhibited lower U_{max}^{C-D} and breakdown strength fields. We note that the much longer charge hold time of a few hundred milliseconds (ms) was applied for C-D measurements than that of 10 ms in P-E, which may have yielded lower U_{max}^{C-D} of the CNETMS films than that in

P-E. Additionally, the microstructural difference in the CNETMS films at varying pH may have contributed to the lower breakdown strength in C-D with the longer charge hold time, in which the longer correlation distance of the CNETMS films catalyzed at $\text{pH} > 2$, i.e., a larger bond angle of siloxane, may have provided low-density domains or channels that facilitated dielectric breakdown with injected charge carriers from electrical contacts.³⁸

Further support for the effect of residual ions in the CNETMS films on overall energy storage performance can be evidenced from the shape of the P-E loops shown in Figure 7. The widened P-E loops of the CNETMS film at pH 1.5 can be correlated with electrical conduction arising from mobile charge carriers inside a dielectric film involving injected charges from electrical contacts and trapped chloride ions that were nearly absent in the CNETMS film at pH 6.5. These charge carriers will be able to accelerate at high electric fields, usually above $300 \text{ V}/\mu\text{m}$ for CNETMS films, which will trigger impact ionization, followed by internal discharge as well as charge carrier multiplication, and eventually the dielectric breakdown of a material.³⁹ Compared to the film at pH 1.5, significantly narrower P-E loops are clearly seen in the CNETMS films catalyzed at $\text{pH} > 2$, which suggests the critical effect of residual chloride ions on energy extraction efficiency.

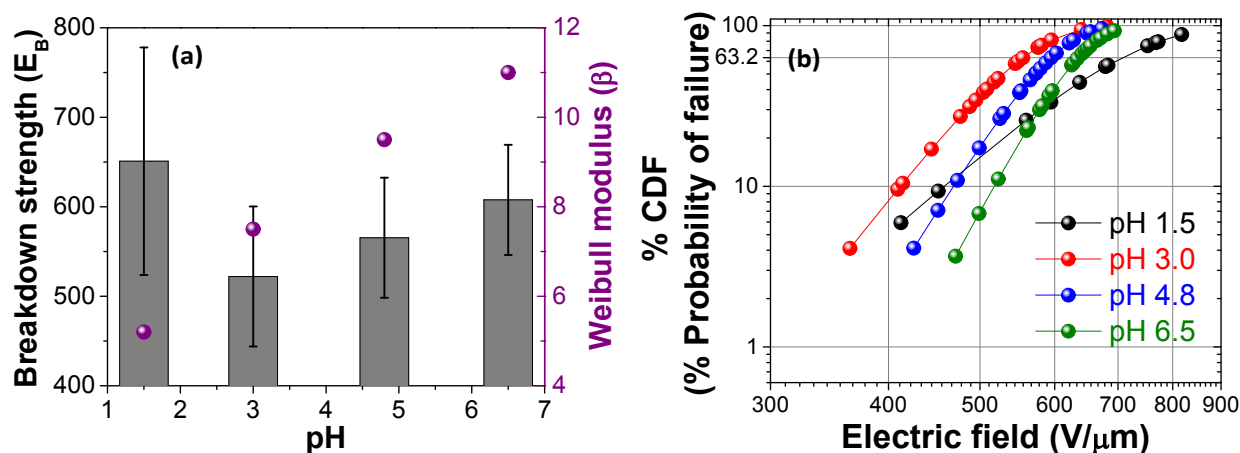


Figure 5. (a) Breakdown strength (in columns) and Weibull modulus (in purple dots) of CNETMS films as a function of pH. (b) % Cumulative distribution function (% CDF) for the probability of electrical failure of the CNETMS.

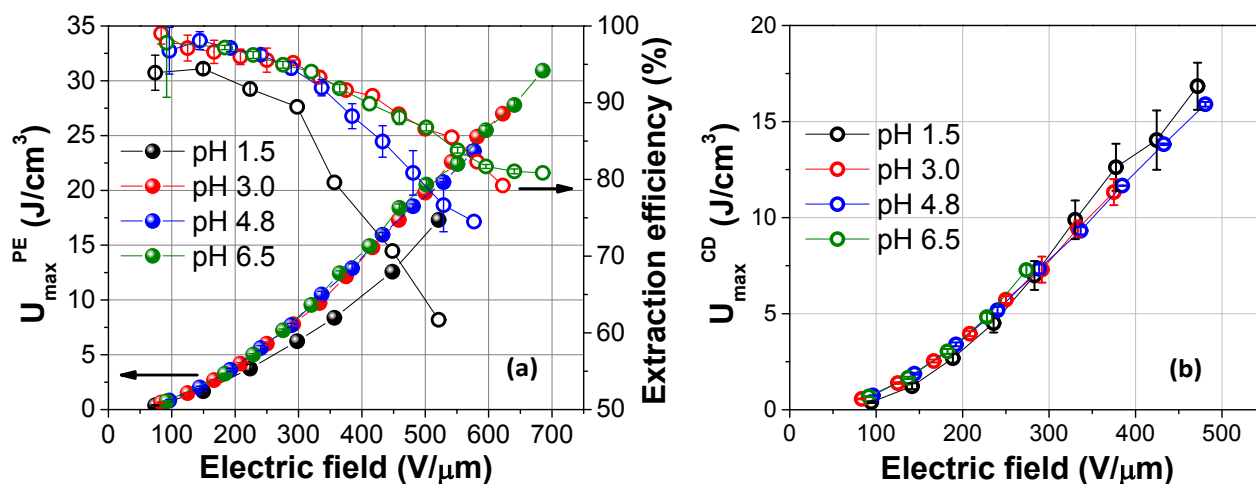


Figure 6. (a) Maximum extractable energy density, U_{max}^{P-E} , (in solid dots) and extraction efficiency (in hollow dots) of the CNETMS films as a function of applied electric field by P-E. (b) Discharged energy density, U_{max}^{C-D} , of the CNETMS films by C-D.

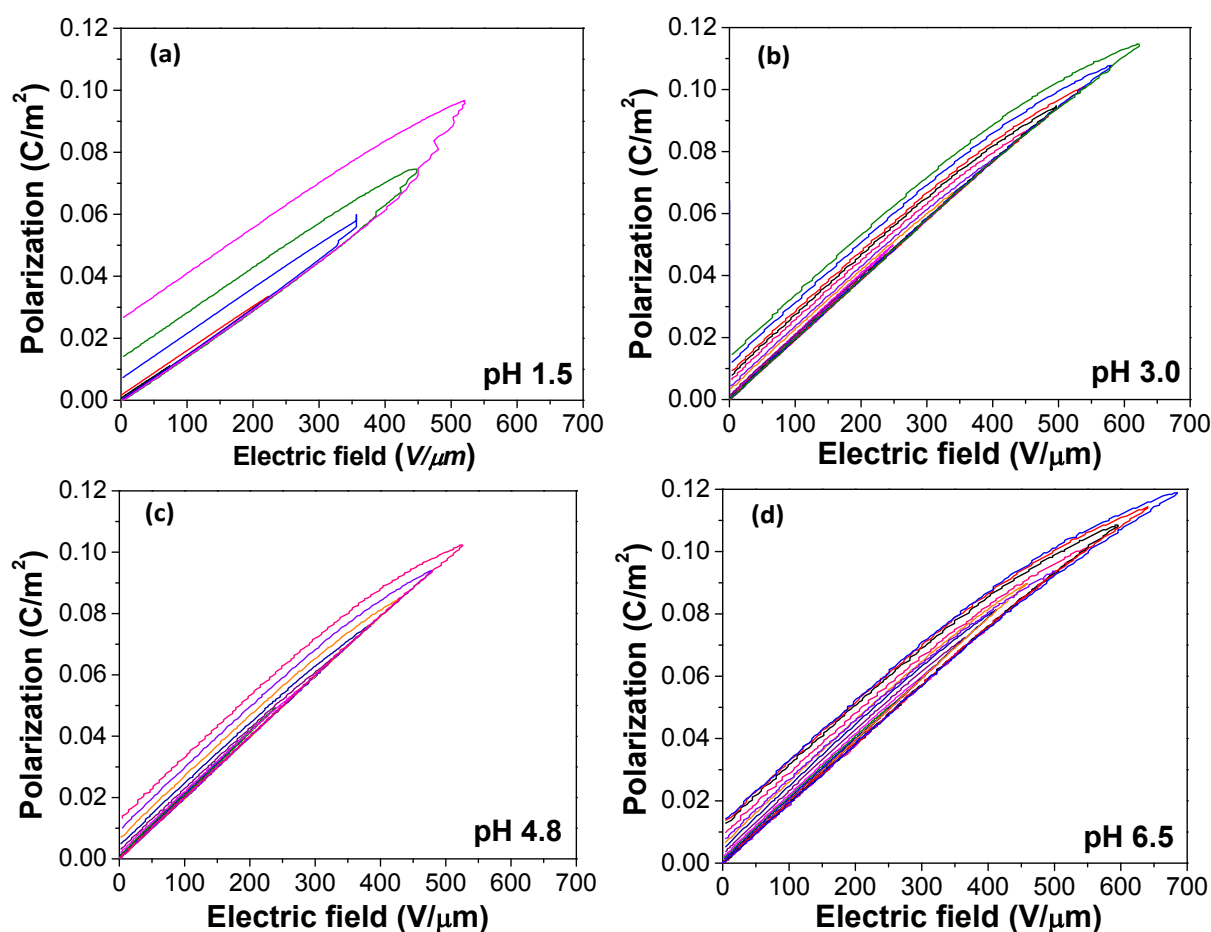


Figure 7. P-E loops of the CNETMS films processed at various pH.

4. Conclusions

In summary, we have shown that the CNETMS film derived from the sol catalyzed at pH 6.5 exhibits an extractable energy density of $32 J/cm^3$ and extraction efficiency of 80% at $685 V/\mu m$ determined by field-dependent P-E measurements. Compared to the CNETMS film processed at pH 1.5, the films at

pH >2 show substantial enhancement in leakage current, breakdown strength, failure reliability, energy density, and energy extraction efficiency. We have correlated the improved dielectric and energy storage characteristics to the reduction and/or absence of residual chloride ions in the films that was used to catalyze the CNETMS sol-gel films, which is believed to restrain any harmful effects of field-activated mobile charges under the influence of high electric field. The excellent failure

reliability along with substantial energy density and extraction efficiency make the CNETMS sol-gel film a suitable material candidate for pulsed power applications.

Conflicts of interest

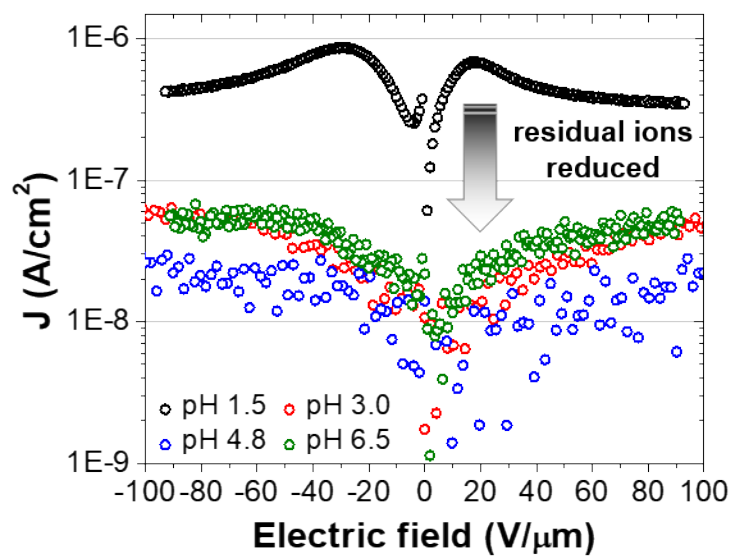
There are no conflicts to declare.

Acknowledgements

This work was supported by the Office of Naval Research Dielectric Films Program (Grant Number: N000141110462) and U.S. Air Force Office of Scientific Research, BioPAINTS MURI Program (Grant No. FA9550-09-0669).

References

1. J. B. Goodenough, H. D. Abruña and M. V. Buchanan, *Basic Research Needs for Electrical Energy Storage. Report of the Basic Energy Sciences Workshop on Electrical Energy Storage*, Report DOE/SC/BES-0702, U.S. Department of Energy (DOE) Office of Science (SC), 2007.
2. Q. Wang and L. Zhu, *Journal of Polymer Science Part B: Polymer Physics*, 2011, **49**, 1421-1429.
3. L. Zhu and Q. Wang, *Macromolecules*, 2012, **45**, 2937-2954.
4. Q. L. K. Han, M. R. Gadinski, G. Z. Zhang and Q. Wang, *Advanced Materials*, 2014, **26**, 6244-6249.
5. E. Baer and L. Zhu, *Macromolecules*, 2017, **50**, 2239-2256.
6. H. Luo, X. Zhou, C. Ellingford, Y. Zhang, S. Chen, K. Zhou, D. Zhang, C. R. Bowen and C. Wan, *Chemical Society Reviews*, 2019, **48**, 4424-4465.
7. Y. Qiao, X. Yin, T. Zhu, H. Li and C. Tang, *Progress in Polymer Science*, 2018, **80**, 153-162.
8. S. Wu, W. P. Li, M. R. Lin, Q. Burlingame, Q. Chen, A. Payzant, K. Xiao and Q. M. Zhang, *Advanced Materials*, 2013, **25**, 1734-1738.
9. O. L. Smith, Y. Kim, M. Kathaperumal, M. R. Gadinski, M. J. Pan, Q. Wang and J. W. Perry, *ACS Applied Materials & Interfaces*, 2014, **6**, 9584-9589.
10. P. Kim, S. C. Jones, P. J. Hotchkiss, J. N. Haddock, B. Kippelen, S. R. Marder and J. W. Perry, *Advanced Materials*, 2007, **19**, 1001-1005.
11. S. A. Paniagua, Y. Kim, K. Henry, R. Kumar, J. W. Perry and S. R. Marder, *ACS Applied Materials & Interfaces*, 2014, **6**, 3477-3482.
12. Y. Kim, O. N. L. Smith, M. Kathaperumal, L. R. Johnstone, M.-J. Pan and J. W. Perry, *RSC Advances*, 2014, **4**, 19668.
13. S. K. Kumar, B. C. Benicewicz, R. A. Vaia and K. I. Winey, *Macromolecules*, 2017, **50**, 714-731.
14. H. Tang and H. A. Sodano, *Applied Physics Letters*, 2013, **102**, 063901-063901-063904.
15. H. Tang and H. A. Sodano, *Nano Letters*, 2013, **13**, 1373-1379.
16. M. A. Wolak, M.-J. Pan, A. Wan, J. S. Shirk, M. Mackey, A. Hiltner, E. Baer and L. Flandin, *Applied Physics Letters*, 2008, **92**, 113301.
17. Z. Xin, C. Qin, Q. M. Zhang and Z. Shihai, *IEEE Transactions on Dielectrics and Electrical Insulation*, 2011, **18**, 463-470.
18. M. Mackey, D. E. Schuele, L. Zhu, L. Flandin, M. A. Wolak, J. S. Shirk, A. Hiltner and E. Baer, *Macromolecules*, 2012, **45**, 1954-1962.
19. X. Zhang, Y. Xu, X. Zhang, H. Wu, J. Shen, R. Chen, Y. Xiong, J. Li and S. Guo, *Progress in Polymer Science*, 2019, **89**, 76-107.
20. J. Jiang, Z. Shen, J. Qian, Z. Dan, M. Guo, Y. Lin, C.-W. Nan, L. Chen and Y. Shen, *Energy Storage Materials*, 2019, **18**, 213-221.
21. P. Kim, N. M. Doss, J. P. Tillotson, P. J. Hotchkiss, M.-J. Pan, S. R. Marder, J. Li, J. P. Calame and J. W. Perry, *ACS Nano*, 2009, **3**, 2581-2592.
22. B. M. Novak, *Advanced Materials*, 1993, **5**, 422-433.
23. J. D. Wright and N. A. J. M. Sommerdijk, *Sol-Gel Materials: Chemistry and Applications*, CRC Press, 2000.
24. J. Chon, S. Ye, K. J. Cha, S. C. Lee, Y. S. Koo, J. H. Jung and Y. K. Kwon, *Chemistry of Materials*, 2010, **22**, 5445-5452.
25. Y. Kim, M. Kathaperumal, O. N. L. Smith, M.-J. Pan, Y. Cai, K. H. Sandhage and J. W. Perry, *ACS Applied Materials & Interfaces*, 2013, **5**, 1544-1547.
26. Y. Kim, M. Kathaperumal, V. W. Chen, Y. Park, C. Fuentes-Hernandez, M.-J. Pan, B. Kippelen and J. W. Perry, *Advanced Energy Materials*, 2015, **5**, 1500767.
27. Y. Kim, M. Kathaperumal, Y. Park, M.-J. Pan and J. W. Perry, *Journal of Materials Chemistry A*, 2017, **5**, 25522-25528.
28. H. Sirringhaus, *Advanced Materials*, 2009, **21**, 3859-3873.
29. X. Zhang, B. Wang, W. Huang, Y. Chen, G. Wang, L. Zeng, W. Zhu, M. J. Bedzyk, W. Zhang, J. E. Medvedeva, A. Facchetti and T. J. Marks, *Journal of the American Chemical Society*, 2018, **140**, 12501-12510.
30. X.-J. She, C. Chen, G. Divitini, B. Zhao, Y. Li, J. Wang, J. F. Orri, L. Cui, W. Xu, J. Peng, S. Wang, A. Sadhanala and H. Sirringhaus, *Nature Electronics*, 2020, 1-10.
31. Z. Zhang, H. Wakabayashi and T. Akai, *Journal of Sol-Gel Science and Technology*, 1998, **12**, 153-158.
32. P. Innocenzi, *Journal of Non-Crystalline Solids*, 2003, **316**, 309-319.
33. J.-L. Bantignies, L. Vellutini, D. Maurin, P. Hermet, P. Dieudonné, M. Wong Chi Man, J. R. Bartlett, C. Bied, J.-L. Sauvajol and J. J. E. Moreau, *The Journal of Physical Chemistry B*, 2006, **110**, 15797-15802.
34. B. Orel, R. Ješe, A. Vilčnik and U. L. Štangar, *Journal of Sol-Gel Science and Technology*, 2005, **34**, 251-265.
35. M. G. Voronkov and V. I. Lavrent'yev, in *Inorganic Ring Systems*, Springer Berlin Heidelberg, Berlin, Heidelberg, 1982, vol. 102, pp. 199-236.
36. Q. Chen, Y. Wang, X. Zhou, Q. M. Zhang and S. Zhang, *Applied Physics Letters*, 2008, **92**, 142909.
37. H. Kakiuchida, E. H. Sekiya, N. Shimodaira, K. Saito and A. J. Ikushima, *Journal of Non-Crystalline Solids*, 2007, **353**, 568-572.
38. K. C. Kao, *Journal of Applied Physics*, 1984, **55**, 752-755.
39. K. C. Kao, *Dielectric Phenomena in Solids*, Academic Press, 2004.



Reduction of residual ions improved overall dielectric properties of an alkoxy silane-based dielectric film, yielding maximum extractable energy density of 32 J/cm³ at 685 V/μm